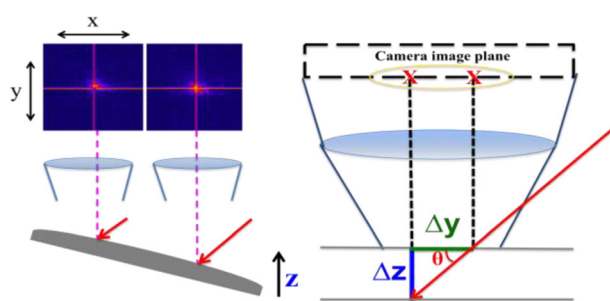


RESEARCH ARTICLE

A Method for Defining the Position of Ion Formation in a MALDI TOFMS by Analysis of the Laser Image on the Sample Surface

Michelle Piotrowski, Brian Malys, Kevin G. Owens 

Department of Chemistry, Drexel University, 3141 Chestnut Street, Philadelphia, PA 19104-2875, USA



Abstract. A method is developed to determine the position of ion formation along the flight axis of a MALDI TOFMS instrument using the image of the laser on the sample surface. Previous work (JASMS 2018, 29, 422–434) showed that misalignment of the sample stage in a Bruker Autoflex III MALDI TOFMS as well as multiple insertions/mountings of the target plate and differences in target plate shape itself produced reproducible changes in the measured ion time-

of-flight which could be attributed to changes in the position of ion formation along the instrument flight axis. Here, a small but reproducible change in the position of the laser in the sample-viewing camera image was observed, with the movement depending on both the sample position and target plate used. Using the change in coordinates of the laser position in the camera image and the known angle of incidence of the laser on the sample surface, the initial z -axis position of the ion at different locations on the plate can be calculated, exactly defining changes in the ion flight path length and the distance between the sample plate and first extraction plate/grid with sample position on the target plate. A correction method is developed to correct the time-of-flight values collected from different locations on the sample plate using the laser images, with the relative standard deviation (RSD) being reduced from 23 ppm to below 6 ppm. The laser images, along with the measured target plate heights, are also used to calculate the misalignment of the sample stage.

Keywords: TOFMS, Electrospray deposition, MALDI, Mass accuracy, Instrument alignment, Sample target plate mapping, MS imaging, Instrumentation

Received: 21 July 2018/Revised: 24 October 2018/Accepted: 29 October 2018/Published Online: 14 December 2018

Introduction

Matrix-assisted laser desorption ionization (MALDI) time-of-flight mass spectrometry (TOFMS) is now widely used in mass spectral imaging experiments. MALDI imaging determines the spatial distribution of molecules as the laser irradiates a surface (like a biological tissue), and signal intensity for the analyte is recorded at specific x/y coordinates [1–6]. TOFMS separates ions by their mass-to-charge (m/z) ratio by

measuring the time it takes for the ions to travel a fixed distance from the source to the detector. The initial position of ion formation determines the overall flight time of the ion in the instrument, as any difference in initial position of the ions along the z -axis results in changes in both the total path length of the ion in the instrument and the magnitude of the electric field in the source. These two effects result in different overall flight times for ions of the same m/z and consequently a decrease in mass accuracy when observing ions formed at different sample locations [7, 8]. The complex nature of imaging samples requires good mass accuracy and mass resolving power. In the case of tissue samples, changes in the morphology and thickness of the samples are known to have an effect on the initial position of ion formation and therefore the absolute ion time-of-flight (TOF) and mass accuracy [3–6].

Electronic supplementary material The online version of this article (<https://doi.org/10.1007/s13361-018-2107-7>) contains supplementary material, which is available to authorized users.

Correspondence to: Kevin Owens; e-mail: kevin.owens@drexel.edu

Previous experiments in our lab performed on a Bruker Autoflex III MALDI TOFMS resulted in poor intensity precision and mass accuracy in the collected spectra [8]. Both the within- and between-sample reproducibility of peak areas were significantly poorer than results seen in previous work. A series of experiments to determine the source of this error was undertaken, with sample preparation, sample deposition, and instrumental and data analysis parameters all investigated. After examining each parameter, no significant improvement in sample signal reproducibility was observed. However, a correlation between peak area, TOF, and sample position on the Bruker 384 MTP target plate was found with the sample position from which spectra were collected having a significant effect on both the measured mass accuracy and intensity reproducibility. Misalignment of the sample stage, multiple insertions and mountings of the target plate, and different shapes of the target plate were the sources of variation of the initial positions of ions created in the source, leading to the error in mass accuracy observed. These results were observed on a total of three Bruker instruments (two Autoflex IIIs and an Autoflex Speed). Each of these sources of variation produced a change in position of ion formation along the z -axis, the axial direction of ions towards the detector, as a function of position on the target plate. Ions formed at different initial positions showed different values of TOF [8]. The errors in mass accuracy seen across the plates were all within the specifications of the three instruments, with mass error all under 200 ppm. A correction was developed to reduce the mass error by a factor of four; the same correction was used to adjust peak area values taken across the plate, significantly reducing the RSD of the sample peak area [8].

In addition to the correlation observed between the sample position on the 384 MTP target plates and the measured TOF, in this work, a relationship between the laser position observed in the sample visualization camera and the sample position was also found. Movement around the target plate showed the laser moving slightly away from and towards the center of the camera crosshairs; this small movement of the laser spot on the surface of the plate also changed reproducibly with different target plates. Using information known about the plate shapes and the sample camera viewing system, a method is developed here to determine the initial position of ion formation at different positions on the sample target plate. This information is then used to correct the measured ion TOF values, leading to significantly improved mass accuracy and precision.

Experimental

Materials

The MALDI matrix alpha-cyano-4-hydroxycinnamic acid (CHCA, > 98%), peptide analyte angiotensin II (ATII, human acetate salt hydrate form, > 90%), polymer analyte polyethylene glycol (PEG) 1000, and cationization agent sodium trifluoroacetate (98%) were obtained from Sigma-Aldrich (St.

Louis, MO) and used as received. Methanol (HPLC grade, 99.9%) was obtained from Fisher Scientific (Waltham, MA). Distilled water was purified in the lab using a Barnstead E-pure system with conductivity of 18 M Ω cm.

Sample Preparation and Deposition

The peptide analyte was prepared by making a 1 mg/mL solution of angiotensin II in water. The CHCA matrix solution was prepared at a concentration of 0.05 M in methanol. A sample solution containing the matrix and angiotensin II was prepared by mixing 2 μ L of the analyte solution with 100 μ L of the matrix solution, yielding a matrix-to-analyte ratio (M/A) of 1295. The polymer analyte and cationization agent were prepared by making a 0.005-M solution in methanol of each. A sample solution was prepared by mixing 150 μ L of the matrix with 1 μ L of the PEG analyte and 1 μ L of cationization agent, which yielded a solution with a M/A of 1000. All samples were deposited onto a Bruker (Bremen, Germany) 384 MTP SS target plate using electrospray deposition (ESD) [9]. Samples were sprayed on locations on the plate that were measured using the depth gage in random order. For ESD, the flow rate was 5.0 μ L/min for 60 s, the spray height was 1.5 cm, and the voltage applied was 5200 V. When just CHCA (0.05 M) was sprayed on the plate, the sample was sprayed with a 2.5 μ L/min flow rate for 1 min. The spray height was 2.0 cm, and the voltage applied was 5300 V.

Plate Measurements

Bruker 384 MTP target plates were used for the collection of TOF measurements and laser images. The x/y dimensions of the plates are 12.4 cm \times 8.2 cm. The plates contain 384 sample wells, where the columns are labeled 1–24 and the rows are labeled A–P, as shown in the diagram in Figure 3a. An Ames 412 depth gage with precision of 2.5 μ m (1/10,000") was used to measure the physical shape of the 384 MTP target plates. Height measurements were taken in rows A, E, I, M, and P and in columns 1, 4, 8, 12, 16, 20, and 24 on each sample target plate.

Collection of Mass Spectra, Sample Images, and Video

Data were collected using a Bruker Autoflex III MALDI TOFMS instrument equipped with a Nd:YAG laser operating at a wavelength of 355 nm. For collection of TOF measurements, the instrument was set in reflectron mode using the Smartbeam 1 setting and the laser intensity set to 16%. The laser repetition rate was 100 Hz, and the laser fired 400 shots for each mass spectrum collected. IS1 was set to 19 kV, IS2 to 16.3 kV, the lens at 8.2 kV, reflectron 1 at 21.0 kV, and reflectron 2 at 9.7 kV. Delayed extraction was used for all experiments with the pulsed ion extraction (PIE) time set to 30 ns. The instrument laser was fired 20 min before the collection of data to allow the laser to warm up. Ten spectra were collected from each sample analyzed. FlexAnalysis ver. 3.4 was used to obtain peak area, TOF, and intensity values.

To collect the images of the laser spots, the same instrument was used with the same settings. The laser was changed to Smartbeam 1, and the intensity was set to 1%. The random walk setting was turned off so that the laser fired in one place. In order to improve the image of the laser in the camera, the sample illumination light in the instrument was blocked using a metal sheet. By doing this, the sample plate inserted into the instrument cannot be seen, only the image of the laser spot on the surface. The laser frequency was set to 200 Hz, and 800 laser shots were collected from the Bruker 384 MTP plate. Once the plate was inserted into the instrument, screen shots of the camera image were captured using Flex control ver. 3.4. However, it was difficult to find the true center of the laser using the screen shots. To improve the image, multiple images of the laser firing were merged together to get a clearer picture of the laser spot. A Hauppauge Impact VCB-e (Hauppauge, NY) model 01381 video capture card was installed in a second computer in order to capture images of the laser spot on the surface. Using Hauppauge Capture ver. 1.1.35054, 4-s long videos with a frame rate of 25 frames/s were collected. Each frame recorded the position of eight individual laser shots. VideoLAN VLC Media player ver. 2.2.5.1 Umbrella was used to extract individual frames from the video.

Images of the laser spot were collected at the same positions where the height measurements of the plates were taken with the Ames depth gage. To reach these positions on the sample plate, the manual fine control was used to input x and y coordinates on the plate. The manual fine control was used to move the plate to ensure all x/y coordinates of the plate were known for every position. Once these positions were typed into the control, the plate is moved by the x/y translation stage. In addition, the x/y coordinates are needed for future calculations of the tilt on the sample stage.

Determination of Laser Spot Location

ImageJ [10] was used to merge multiple video frames collected from each plate position to find the center of the laser image. Only seven pictures at a time can be merged in ImageJ. As expected, the more frames that are merged, the error in finding the center of the spot between images is reduced. To find the center of the laser spot, the threshold tool in ImageJ is used to highlight the laser spot. By adjusting the threshold, pixels of a certain intensity are isolated from the other pixels in the image. The center point of the laser spot is found taking the average of the x and y coordinates of the pixels selected. It was found that no more than 21 frames needed to be averaged as the standard deviation for the pixel coordinates remains around 0.26 pixels or 0.60 μm after the x/y pixel center is converted to absolute position.

Image Calibration to Absolute Position

Once the x/y coordinates for the center of each laser spot are found, the pixel values need to be converted to absolute position in microns (μm) so that the distance between each laser position can be found. To convert pixels to μm , an image with a

known distance is needed for calibration. The image must be collected the same way the data is collected to ensure the images have the same number of pixels and magnification. All of the frames collected using the VLC Media player were 720×576 pixels in size. To obtain an image for calibration, a sample of CHCA matrix alone was deposited onto plate A by ESD. The sample was loaded into the instrument, and a video was taken after the laser was fired multiple times at specific coordinates in the sample well with the random walk setting turned off. This ensured the continuous firing of the laser on the same position so the matrix is fully ablated from the sample surface. Each laser spot was 300 μm apart in the x direction and 200 μm apart in the y direction. In order to ensure that the distance the plate moved was correct, microscope images of the plate after analysis in the instrument were also collected. Since the distance between the spots was known, using the line and scale functions in ImageJ, it was possible to determine the number of pixels/ μm . Once that value was found, the center of the laser spots measured was converted from pixels to absolute position in μm .

Results and Discussion

Figure 1a shows a photograph taken of the sample stage setup of the Bruker AutoFlex TOFMS. The target plate holder and the x/y translation stage can be clearly seen. Figure 1c shows a simplified schematic diagram of a TOF source. The surface of the target plate is G0, and z is the axial direction of ions towards the detector. Figure 1b shows two of the three adjustment screws which mount the target plate holder to the x/y translation stage. The three screws are used to set both the planarity of the plate and the absolute distance (D1) between the target plate and the first grid/extraction plate (G1) in the instrument as shown in Figure 1c. Misadjustment of these screws would result in a tilt of the target plate holder in either or both of the x and y directions, resulting in different z positions for ions formed from different sample locations on the target plate. The different z values at different positions on the sample plate create different D1 values for the ions, resulting in flight time differences due to changes in both the path length of ions to the detector and the magnitude of the electric field in the region D1. This was demonstrated in our earlier work by evaluating the TOF measurements observed from different positions on the sample plates on three different instruments [8]. The TOF measurements also changed when different plates were used due to the shape of the different plates [8]. Supplemental Figure S1 shows the measured plate heights for the four MTP target plates labeled plates A, B, F, and M used in this work. The measured heights are not absolute values as they have been normalized by subtracting the minimum value of the height measured for that plate. Note that plates A and F have a convex shape, which is a typical shape observed for other plates in our lab. However, plate B shows a relatively planar but slanted shape, and plate M shows a tilted convex shape. These differences in plate shape and the misalignment of the sample stage

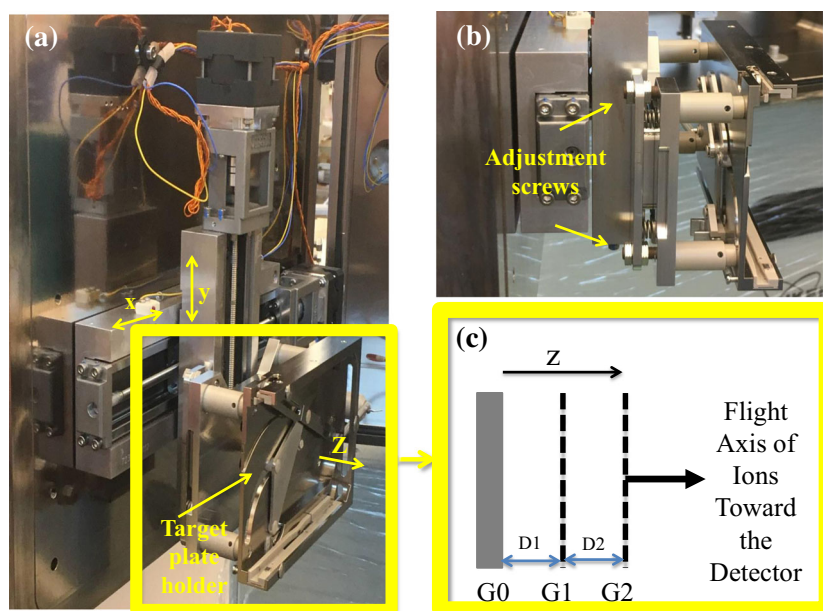


Figure 1. Photographs of the stage setup for the Bruker Autoflex instrument. (a) The target plate holder and the x/y translation stage. (b) Close-up of the target plate holder showing two of the three adjustment screws used to set the plate planarity. (c) Schematic diagram of the TOF source, where G0 is the sample target plate and G1 and G2 are the first and second grid/extraction plate. D1 is the distance between the target plate G0 and the first grid/extraction plate, while D2 is the distance between the grids/extraction plates G1 and G2

were the major sources of error observed when comparing sample-to-sample reproducibility in our previous work [8]. Differences in shape of the plate lead to larger errors when using external calibration [8, 11, 12]. In addition, mounting the target plate to the base plate and loading the plate into the instrument also contributed to the change in z and therefore a change in flight time. A more detailed explanation of the relationship between measured TOF and sample stage misalignment and plate shape can be found in reference [8].

Movement of the Laser

In addition to the correlation seen between the sample position on the 384 MTP target plate and the measured TOF, a relationship between the laser position observed in the sample viewing camera and the sample position was also found. This is illustrated in Figure 2a where several screen shots taken with the Bruker sample-viewing camera observe different sample positions on target plate A. The first box in Figure 2a shows the image taken at the left side of the plate in position E1. The laser spot is observed in the upper-right quadrant of the cross hairs in the camera image. Moving across the plate from left to right, the laser moves from that position in the upper-right quadrant to the center of the cross hairs as seen in the far-right box showing the image collected from position E24. Using ImageJ, the center x/y pixel coordinates of the laser spots were found, and Figure 2b shows the y values of the laser image as a function of the sample position on the plate. Looking at the change in laser position for all four plates, the center x/y pixel coordinates of the laser spots were found to be changing moving across the rows and down the columns on the sample

plate. Figure 2c shows the change in x/y coordinates across row A for plates A, B, F, and M.

One of the reasons for the change in laser position in the camera image is due to misalignment of the sample stage. Figure 3 shows a schematic of the laser and camera visualization system used in the Bruker Autoflex instrument to illustrate this situation. Figure 3a shows the ion source, where the target plate is inserted into the front of the instrument. The “cloverleaf pattern” at the top of the diagram illustrates the openings in the G1 source plate; ions are extracted through the small central opening, while the desorption laser, camera, and sample illumination light enter through three of the non-central four openings shown. Note that the camera and the laser are stationary and are located at right angles to each other; further, the laser and the camera optics are viewing the plate at an angle of 60° . As the laser is hitting the plate at an angle, any change in height along the z -axis will result in a change in the position of the laser in the camera image. Figure 4b shows a side view of the target plate and the sample holder in the source, which are moved by the x/y translation stage to get to different sample positions located on the plate. As the plate is moved to different positions by the x/y translation stage, the camera images the laser spot as it hits the plate. When both the sample stage and target plate are flat, the position of the laser with respect to the camera optics does not change as the plate is moved to different sample positions.

Figure 4 illustrates what is observed if the sample plate exhibits a difference in height along the z -axis when looking at sample positions 1 and 2. The laser hits the plate at different heights, and the camera images a different position of the laser spot on the surface. This difference in the z -axis position will be

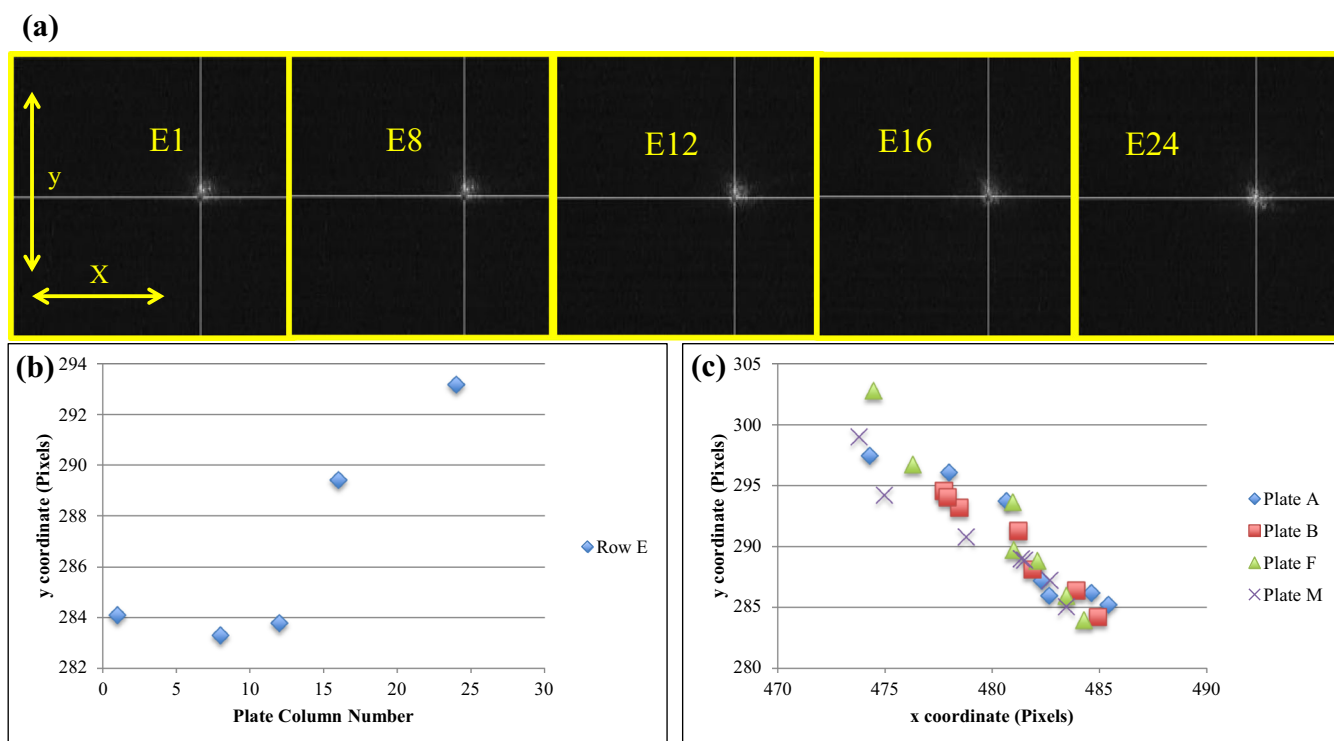


Figure 2. (A) Screen shots of the laser position taken using the instrument camera while moving across row E on plate A. (B) The y values of the laser position as a function of plate position calculated from the photos shown in panel A. (C) y pixel positions correlated with the x pixel positions for row A on plates A, B, F, and M

seen in the camera image, where the laser is observed at a different x/y coordinate in the image as the plate is moved from position 1 to 2. Figure 4a shows a simplified picture of the camera optics and the sample plate at two different positions.

As the laser hits the sample at position 1, the camera captures an image of the laser, with the laser shown in the center of the cross hairs in Figure 4b in a top down perspective. When in position 1, the laser is centered in the cross hairs, but as the

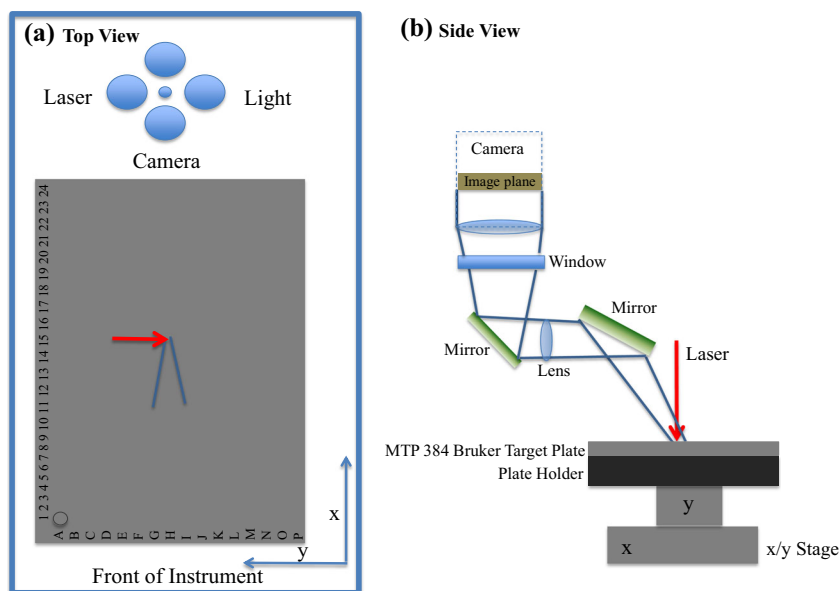


Figure 3. (A) Schematic diagram of the top view of the instrument source, as the target plate is loaded into the front of the instrument. The “cloverleaf pattern” at the top illustrates the openings in the G1 source plate; ions are extracted through the small central opening, while the desorption laser, camera, and sample illumination light enter through three of the non-central four openings. (B) Side view of the x/y stage, plate holder, and loaded target plate. The laser enters from behind the plane shown; the in-plane path of the camera view of the instrument is shown

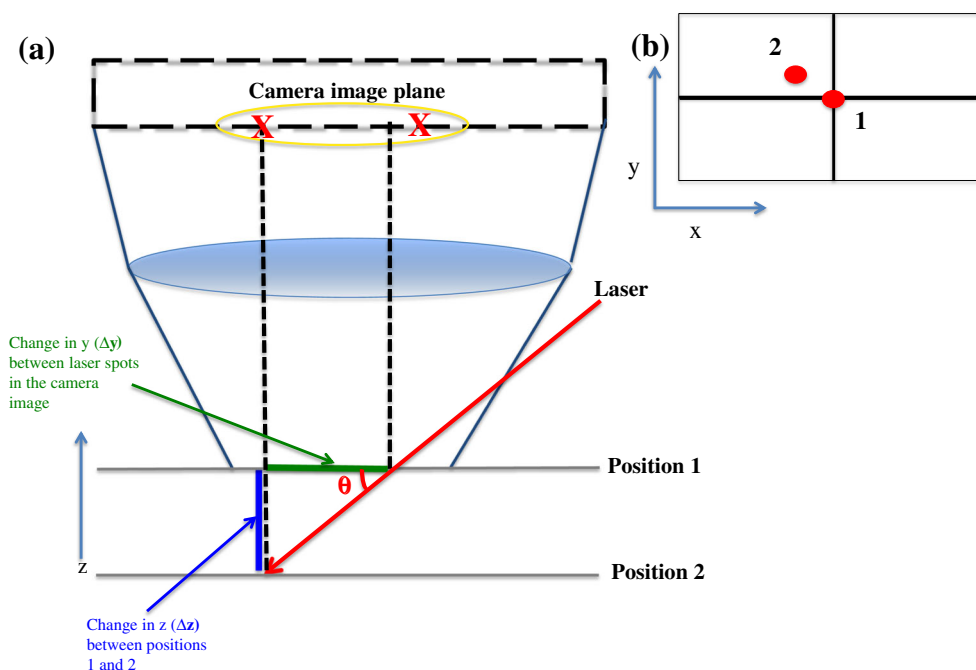


Figure 4. (a) Side view of the sample plate located at two different z positions, including a simplified view of the lens and camera image plane. Positions 1 and 2 represent different heights of the plate. As the laser comes in at an angle of 60° to the surface, the camera images a different position of the laser on the surface. (b) Shows a top-down view of the in-camera image with cross hairs. The laser spot appears centered in the cross hairs when the plate is at position 1, but as the z position changes, the camera images a different x/y coordinates of the laser for position 2

height of the plate changes, the camera images a different x/y coordinate of the laser at position 2. Position 2 has a different height z due to either a tilt on the sample stage or due to the shape of the target plate. As the laser hits the plate at position 2 at the same angle, the image of the laser spot is observed to shift away from the center of the cross hairs.

Figure 4 demonstrates what happens to the camera image with the differences in z position where these differences are due mainly to the misaligned sample stage and the unique shape of the plate being used. As shown in Supplemental Figure S1, each plate has a unique shape that will contribute to the initial position of ion formation. Figure 5 shows the measured TOF values and y pixel coordinates of the laser taken when analyzing an electrosprayed sample of CHCA and angiotensin II deposited on plate F. When plotting the y values of the laser center versus sample position on the plate, it can be seen that the laser follows the same pattern seen in the TOF data. Moving left to right across, the plate for rows E and M (data from columns 4, 8, 12, 16, and 20) shows an increase in flight time. This suggests a misalignment of the sample stage going from left to right (in agreement with the misalignment seen with plates A and B in reference [8]). The left of the sample stage has a higher z position of ion formation compared with the right of the sample stage because a higher height would result in shorter TOF values, with the initial position of ions forming closer to the detector (and similarly a lower height would result in a longer TOF, because the ion initial positions are farther away from the detector). Ions forming at the left side of the sample plate (with higher initial z position)

experience a shorter distance $D1$ between the surface of the target plate ($G0$) and the first grid/extraction plate ($G1$) in the instrument source, while those formed on the right side of the sample plate (with lower initial z position) experience a longer distance $D1$ between $G0$ and $G1$. Note that the flight times show the inverse of the slightly tilted convex shape of plate F (as shown in Supplemental Figure S1). The TOF measurements therefore show a combination of plate shape and misalignment of the sample stage, where there is a tilt and a concave shape observed in the measured flight times at the different positions. The laser coordinates for plate A shown in Figure 2b also show the inverse of the shape of plate A, which has a convex shape. The laser position also changes in moving across the plate in the same way that the flight time measurements change, similarly reflecting the misalignment of the sample stage and the shape of the plate used.

Defining the z Position

Figure 2c shows the x/y center coordinates of the laser spots for plates A, B, F, and M moving across row A. If the sample stage and plates were flat, at every sample position, the laser would have the same coordinates, which is not what is observed. As demonstrated previously with Figure 2, there is movement in the laser position in moving to different positions on the target plate, with the center of the laser image having different coordinates (in pixels). This visual change moving across the row shows that there is a tilt on the sample stage moving from left to

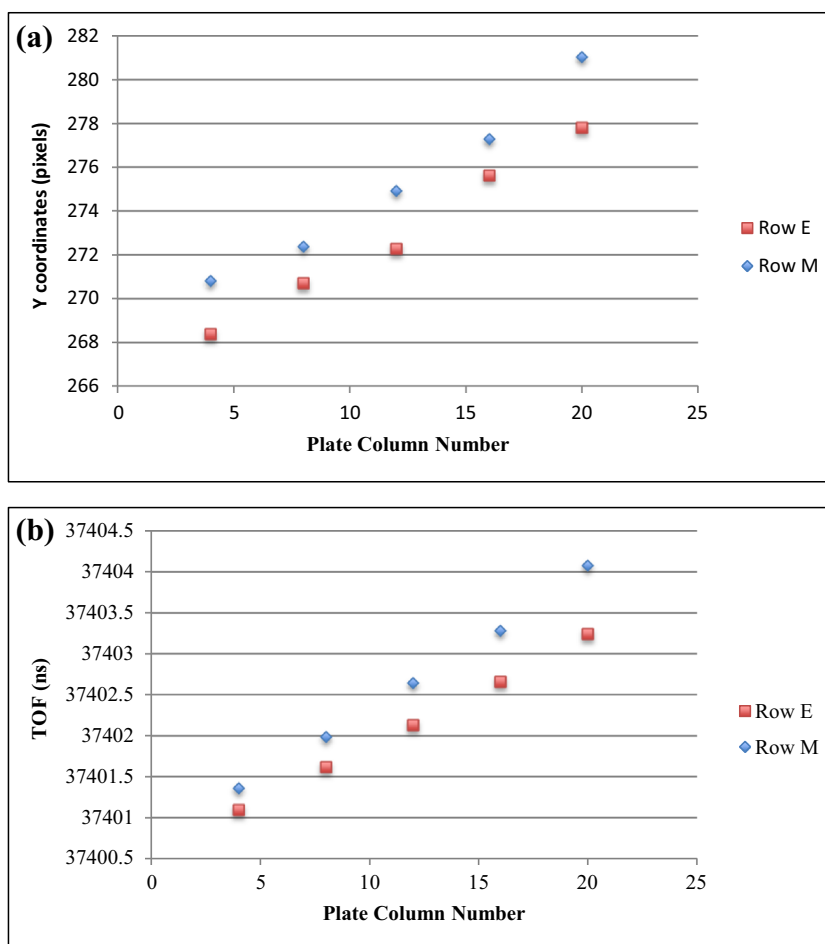


Figure 5. (a) y coordinates of the laser spots, and (b) measured flight times for angiotensin II (in CHCA matrix) taken in rows E and M columns 4, 8, 12, 16, and 20 on plate F. The samples were deposited by electrospray deposition

right (i.e., in the x direction). The information found from the changing y coordinates of the laser can be used to find the height z of the sample plate at different the positions. Figure 4a shows a simplified model of the laser hitting the plate at two positions. The difference in the height of the plate between the two positions is called the change in z (Δz). When the laser hits the plate at the two different positions, the camera images the laser spot on the surface at different x/y coordinates. Figure 4a shows the distance between the laser spot in the camera image in the y direction. The difference in y (Δy) can be used to find the Δz at different positions on the plate because the angle of the laser with respect to the surface is known. The change in height z can be found using the trigonometric function given by Eq. (1):

$$\Delta z = \tan \theta \cdot \Delta y \quad (1)$$

In order to calculate the z values, the y coordinates of the laser spot are needed. Once the coordinates are found, these values must first be converted from pixels to microns. Table 1 shows a list of the y values for plate A. To find Δy , each of the y values is first subtracted from the y value of a chosen reference position on the plate. Sample position A1 is the reference

position chosen for all the values shown in Table 1. These values are then plugged into Eq. (1) and combined with the angle of the laser (which in the Bruker instrument is 60°) to give the Δz value for each sample position shown. When investigating multiple loadings of the plate and comparing Δz values, it was found that the standard deviation ranged from 1 to 3 μm depending on the sample position on the plate. This is shown in Table 2, showing the calculated Δz for plates A and F where the plates were loaded into the instrument five times.

Using the camera image of the laser and the angle of the laser the initial z position in which the ions are formed can be found at different x/y positions of the sample stage. Figure 6 shows the calculated value of z for row A of the four different plates compared to the measured height for row A of each plate. The z values represent the difference in height z at each sample position shown. As stated previously, both the misalignment of the sample stage and the shape of the plate both contribute to the z position from which the ions are formed. Figure 6 demonstrates that the calculated z values show a combination of plate shape and sample stage tilt. This method can be used to calculate the initial position of ion formation on instruments with a similar instrument source set up to the Bruker Autoflex III. However, in order for this method to work, the laser must intersect the target

Table 1. The Measured y and Calculated Δy (Using Plate Position A1 as the Reference) and Δz Values for Plate A at Different Sample Positions

Plate position	y (um)	Δy (um)	Δz (um)
A1	606.1	0.0	0.0
A4	610.1	-4.0	-7.0
A8	614.4	-8.3	-14.3
A12	617.9	-11.8	-20.5
A16	626.6	-20.4	-35.4
A20	632.2	-26.1	-45.2
A24	639.1	-33.0	-57.2
I1	616.3	-10.1	-17.6
I4	624.6	-18.5	-32.0
I8	617.5	-11.4	-19.7
I12	621.2	-15.1	-26.1
I16	629.1	-23.0	-39.8
I20	631.4	-25.3	-43.9
I24	646.2	-40.0	-69.3
P1	616.9	-10.8	-18.7
P4	616.5	-10.4	-18.0
P8	615.6	-9.5	-16.4
P12	617.6	-11.5	-19.9
P16	627.3	-21.2	-36.7
P20	647.6	-41.4	-71.8
P24	652.3	-46.1	-79.9

plate at an angle, so the change in height is converted into movement of the laser spot in the camera image.

For the Bruker Autoflex III instrument used in this work and in reference [8], a misalignment of the sample stage (resulting in different z positions of the ions) led to a decrease in mass accuracy and sample reproducibility when collecting data from different x/y coordinates on the sample plate [8]. By measuring the z position using the laser on the instrument, a mechanism to control the sample stage in the z direction could be implemented into the TOF instrument. Using the laser to calculate the height at every sample position, adjustments could be made to the sample stage, depending on the topography of the sample and location of the sample on the plate. Controlling the sample stage in the z direction would enable the user to control the initial position of the ions formed. This would decrease the

Table 2. The Calculated Mean and Standard Deviation of Δz for Five Insertions of Plates A and F into the Instrument

Plate	Spot	Mean (um)	SD (um)
A	E8	-1.8	0.7
A	E12	-7.7	1.9
A	E16	-16.2	1.8
A	E20	-25.3	2.4
A	M4	-5.2	2.0
A	M8	-3.2	1.8
A	M12	-9.6	1.6
A	M16	-22.5	2.6
A	M20	-37.3	3.0
F	E8	-9.7	1.2
F	E12	-22.2	2.8
F	E16	-31.6	2.7
F	E20	-40.3	2.4
F	M4	-9.5	0.1
F	M8	-15.3	0.4
F	M12	-26.8	0.6
F	M16	-36.0	0.5
F	M20	-52.2	1.5

observed mass error of samples. In addition, it could make analyzing a sample that varies in height at different positions (like a piece of tissue) easier, where the sample stage could be moved up or down in the z direction to improve the mass accuracy of the sample.

Correction of TOF Measurements Using the Δz Values

At different sample positions on the plate, the misalignment of the stage and plate shape causes a reproducible change in TOF values. Note the calculated Δz is the initial position at which the ion forms, and therefore represents a change in the distance $D1$ from the sample plate surface to the first grid/extraction plate. In comparing the TOF for samples located at different sample spots, there is a loss of mass accuracy and decrease in reproducibility of flight times. Table 3 shows the Δz position found from the Δy coordinate of the laser and the ΔTOF measurements for angiotensin II taken from row E on plate F. Comparing the two values shows the same ratio of $\Delta TOF/\Delta z$ at different sample positions on the plate. Using this information, the observed laser position can be used to predict the change in flight times across and down a plate, and a linear correction can then be used to adjust the measured TOF.

TOF measurements must be corrected for the change in initial position due to sample location on the plate (C_{posx}) and also for different insertions of the sample plate into the instrument (C_{insx}). A standard solution must be electrosprayed on the same sample position on the plate, and the mean TOF for a given m/z is taken from this sample for every plate insertion. One of the insertion TOF values are chosen as the reference set ($TOF_{\text{posx,ref}}$) used to calculate C_{insx} . The correction process is demonstrated with Tables 3, 4, and 5, using four different samples of CHCA and angiotensin II sprayed on plate F on the sample locations E4, E8, E12, E16, and E20.

The first step in the correction is to find $R_{\Delta TOF/\Delta z}$, which will be used to calculate the set of C_{posx} values. Table 3 shows that the randomly chosen spot E12 is used to calculate the ratio between the change in flight times and change in z , $R_{\Delta TOF/\Delta z}$ (note that while the units for $1/R_{\Delta TOF/\Delta z}$ are distance divided by time, this should not be interpreted as an absolute velocity or change in velocity for ions formed at different z -axis locations in the source). Only one spot is needed for this calculation because the ratio is found to be constant from spot to spot on the plate. The value, $R_{\Delta TOF/\Delta z}$, used to calculate C_{posx} as shown in Table 3, is $0.045 \text{ ns}/\mu\text{m}$. To find the set of corrections for each position on the target plate, the Δz from each position is multiplied by $R_{\Delta TOF/\Delta z}$ as shown in Eq. (2):

$$C_{\text{posx}} = \Delta z_{\text{posx}} \times R_{\Delta TOF/\Delta z} \quad (2)$$

where C_{posx} is the correction for each plate position and Δz_{posx} is the change in z for a particular plate position. The results of applying Eq. (2) are shown in Table 3 to calculate the different C_{posx} values for sample spots across row E. The table shows each Δz for each spot position being

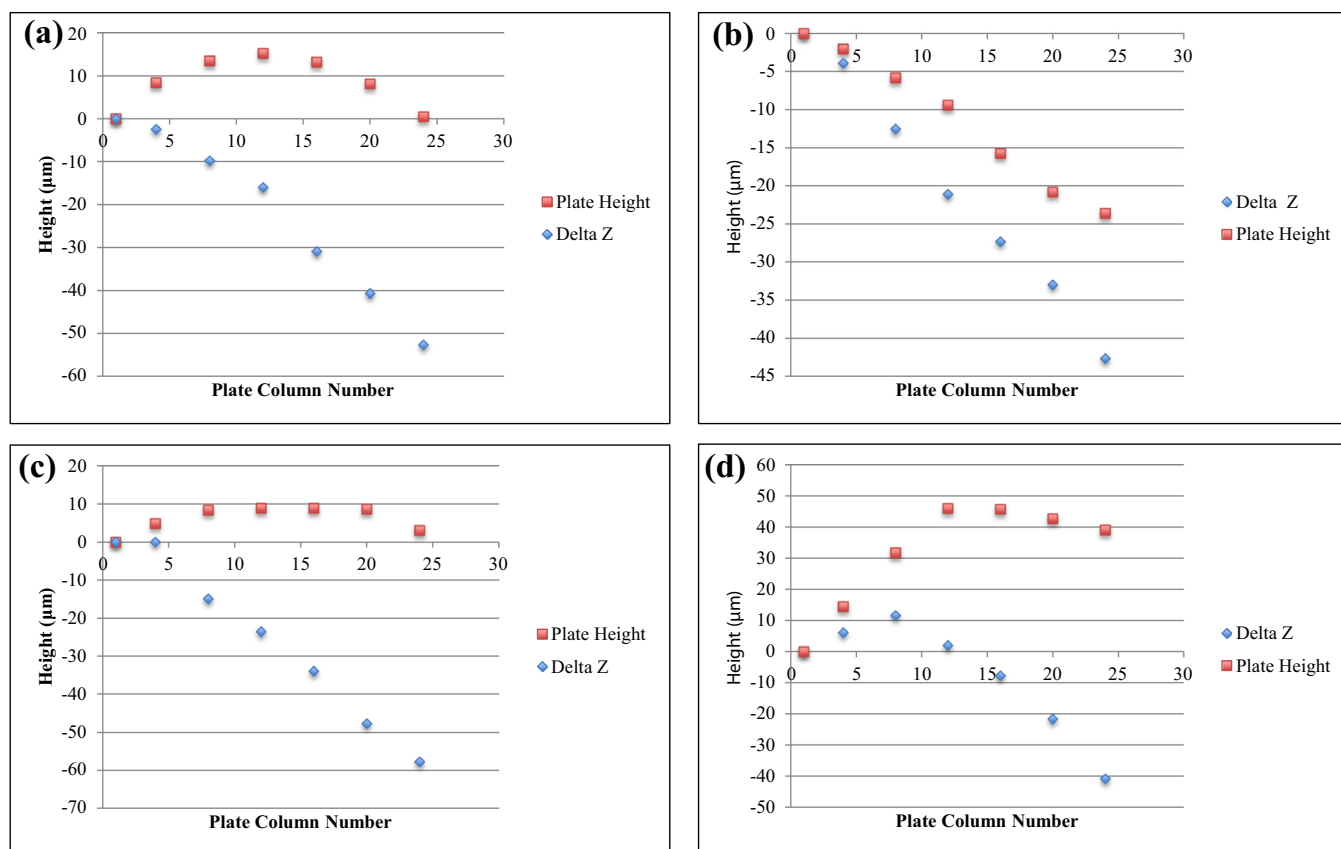


Figure 6. Plots of calculated Delta z values for (a) plate A, (b) plate B, (c) plate F, and (d) plate M, along with the measured plate heights for row A of the plates. A combination of the tilt of the stage and the shape of the plate can be seen in the calculated Delta z values

multiplied by the $R_{\Delta\text{TOF}/\Delta z}$ 0.045 ns/μm to yield the C_{posx} values for each spot.

To correct for multiple loadings into the instrument and mountings of the base plate, a second correction is needed. The same sample solution is electrosprayed on the same sample position on the plate, and the mean TOF is taken from this sample. Of the multiple insertions, one is selected as the reference data set. Each insertion of the target plate will have its own correction factor as shown in Eq. (3):

$$C_{\text{ins}} = \text{TOF}_{\text{posx,ref}} - \text{TOF}_{\text{posx}} \quad (3)$$

Table 3. The Calculated Change in z Position (Δz) and the Change in Average Flight Times for Angiotensin II (in CHCA Matrix) on Plate F at Different Sample Positions in Row E

Spot	Δz (μm)	Mean ΔTOF (ns)	$\Delta\text{TOF}/\Delta z$ (ns/μm)	C_{posx}
E4	0	0	–	0
E8	–11.6	–0.5	0.043	–0.5
E12*	–22.4	–1.0	0.045 ($R_{\Delta\text{TOF}/\Delta z}$)	–1.0
E16	–35.4	–1.6	0.045	–1.6
E20	–41.2	–2.2	0.046	–1.8
		Mean	0.045	
		SD	0.0012	

The mean and standard deviation are shown for the ratio between the TOF and Δz position. Note that the ratio between the ΔTOF and the laser Δz position for each sample position remains constant. The correction for each position on the plate (C_{posx}) is calculated using Eq. (2) with $R_{\Delta\text{TOF}/\Delta z}$ found at spot E12

where $\text{TOF}_{\text{posx,ref}}$ is the selected reference set, the TOF values from a chosen insertion to correct the data from other insertions. TOF_{posx} is the average TOF taken from each loading into the instrument. Table 4 shows the average TOF measurements from spot E4 for four insertions of the target plate into the instrument and the calculation of C_{ins} for each insertion, with insertion 1 chosen as $\text{TOF}_{\text{posx,ref}}$.

Once C_{posx} and C_{ins} are calculated, they can be used to correct the raw TOF values measured at different positions on the plate. Table 5 shows the TOF and mass measurements taken from five spots and four different insertions. The TOF measurements are corrected using Eq. (4):

$$\text{TOF}^* = \text{TOF}_{\text{posx}} + (C_{\text{posx}} + C_{\text{ins}}) \quad (4)$$

where TOF^* is the corrected flight time calculated from the measured TOF from position x on the plate (TOF_{posx}). The

Table 4. The Average TOF Measurements for Angiotensin II in CHCA Sprayed on Plate F Spot E4 for Four Insertions into the Instrument

Insertion	Spot	Mean TOF (ns)	C_{ins}
1	E4 ($\text{TOF}_{\text{posx,ref}}$)	37,398.2	0
2	E4	37,397.8	0.4
3	E4	37,398.9	–0.7
4	E4	37,398.8	–0.6

The correction for each insertion into the instrument (C_{ins}) is calculated using Eq. (3) using insertion 1 as the reference set

Table 5. The Uncorrected (TOF/ m/z) and Corrected (TOF*/ m/z^*) Time of Flight and Mass-to-Charge Measurements for Protonated Angiotensin II in CHCA Taken from Four Different Sample Spots on Plate F and Four Different Plate Insertions

Insertion	Spot	TOF (ns)	m/z	C_{posx} (ns)	C_{insx} (ns)	TOF* (ns)	m/z^*
1	E4	37,398.2	1046.490	0.0	0.0	37,398.2	1046.490
1	E8	37,398.7	1046.521	-0.5	0.0	37,398.2	1046.490
1	E12	37,399.2	1046.544	-1.0	0.0	37,398.2	1046.485
1	E16	37,399.8	1046.581	-1.6	0.0	37,398.2	1046.488
1	E20	37,400.1	1046.613	-1.8	0.0	37,398.3	1046.505
2	E4	37,397.8	1046.469	0.0	0.4	37,398.2	1046.492
2	E8	37,398.3	1046.498	-0.5	0.4	37,398.2	1046.490
2	E16	37,399.4	1046.559	-1.6	0.4	37,398.2	1046.488
2	E20	37,400.0	1046.592	-1.8	0.4	37,398.6	1046.506
3	E4	37,398.9	1046.476	0.0	-0.7	37,398.2	1046.489
3	E8	37,399.5	1046.508	-0.5	-0.7	37,398.3	1046.490
3	E12	37,400.1	1046.542	-1.0	-0.7	37,398.4	1046.496
3	E16	37,400.6	1046.569	-1.6	-0.7	37,398.3	1046.489
3	E20	37,401.2	1046.604	-1.8	-0.7	37,398.7	1046.508
4	E4	37,398.8	1046.470	0.0	-0.6	37,398.2	1046.491
4	E8	37,399.3	1046.500	-0.5	-0.6	37,398.2	1046.490
4	E12	37,399.9	1046.532	-1.0	-0.6	37,398.3	1046.494
4	E16	37,400.4	1046.561	-1.6	-0.6	37,398.2	1046.488
4	E20	37,401.0	1046.594	-1.8	-0.6	37,398.6	1046.506
	Mean	37,399.5	1046.538		Mean	37,398.2	1046.493
	SD	0.94	0.046		SD	0.16	0.010
	RSD (ppm)	25.02	43.75		RSD (ppm)	4.3	6.90

The C_{posx} and C_{insx} are shown for each spot and insertion

TOF* for each spot and insertion is shown in Table 5. Note that before the correction is applied, each set of TOF data showed a relative standard deviation (RSD) of around 25 ppm. After the correction was applied, the RSD of the TOF values dropped to ~4 ppm, and the RSD of the mass measurements across the plate was reduced to ~7 ppm. Sample set 1 and insertion 1 were used to calculate the correction for insertion and position for the different sets of data.

As a demonstration of the generality of the correction, this process was also applied to different oligomers of a sample of PEG 1000 with CHCA as the matrix using the correction values found from the TOF values of angiotensin II. The PEG sample was sprayed in the same five spots on plate F as angiotensin II, and the plate was loaded into the instrument twice. The RSD for TOF of the degree of polymerization (DP) = 23 oligomer (at $m/z = 1053$) was reduced from 23 to 3 ppm after correction. Applying the angiotensin II correction to other oligomers (DP = 17, 20, 25, and 29), the TOF RSD was reduced from ~23 ppm to below 6 ppm. Note that the RSD of corrected TOF values increases for the lower and higher m/z oligomers of the PEG.

To further investigate how the correction factors (C_{pos} and C_{ins}) change with m/z , separate sets of correction values were calculated for five different oligomers of PEG 1000. The calculated $R_{\Delta\text{TOF}/\Delta Z}$ and correction values for 2 loading into the instruments are provided in Supplemental Table S1. Each oligomer of PEG had a slightly different $R_{\Delta\text{TOF}/\Delta Z}$, with the ratio increasing as the m/z value increased, resulting in an increase in the C_{pos} and C_{ins} values. Supplemental Figure S2 shows the average $R_{\Delta\text{TOF}/\Delta Z}$ for the five oligomers of the PEG sample as a function of the degree of polymerization. The increase in $R_{\Delta\text{TOF}/\Delta Z}$ with the increase in m/z is found to be

linear, where the equation of the line given can be used to calculate $R_{\Delta\text{TOF}/\Delta Z}$ for different m/z values.

As a further example, the correction values from the DP = 23 oligomer were applied to the five different oligomers; as expected from application of the angiotensin II correction factors, the RSD value increased as the m/z ratio moved farther away from that of the DP = 23 oligomer, as shown in Supplemental Table S2. The table shows the average TOF and mass measurements (both uncorrected and corrected) taken from the five spots across the plate. Although the error of the corrected peaks increased as compared to using individual correction factors for each different oligomer, the RSD was still reduced by a factor of ~4X. Supplemental Table S2 also shows the uncorrected and corrected mass measurements for the five oligomers corrected using the correction values from DP = 23 oligomer. The RSD of the mass measurements across the plate is still reduced by a factor of 3X or more.

Calculating the Misalignment of the Sample Stage

Another application of finding the height at each position of the plate is to calculate the tilt of the sample stage. In order to measure the tilt of the sample stage, height measurements for the plate are needed for every position in which a video of the laser spot was taken. The tilt of the sample stage can then be calculated by finding the equation of a plane using the x , y , and z coordinates determined using the least squares method. The x and y coordinates needed are the values input into the instrument to move the sample stage to different positions. Using the z measurements determined at each position, the equation of a plane can be calculated to find the tilt across a row and down a column of a plate. First, the calculated z values must be

adjusted by subtracting the plate shape so that when the equation of the plane is found, the z will only account for the tilt of the sample stage. To subtract the plate shape, the measured height at position A1 is subtracted from every height measurement taken at the various positions. Then, these values can be subtracted from the Δz values. Once the adjusted z values are found, they can be used to calculate the equation of the plane.

A least squares method is used to fit the x , y , and z points to find the equation of the plane $z = Ax + By + C$ [13]. Once the equation is calculated, it can be used to calculate the height z (μm) for any position the sample plate can move to. Figure 7a shows the calculated tilt for all the rows of plate A using the equation found using the least squares method. The tilt found across the rows is approximately $50 \mu\text{m}$. Figure 7b shows the tilt of the sample stage going down a column for rows A, E, I, M, and P, which is approximately $7 \mu\text{m}$. To test the other plates, the equation of the plane was calculated using the data collected from plates B, F, and M. These equations are also recorded in Table 6. Comparing the calculated values of the tilt for each plate, the average tilt across the row is found to be $50 \mu\text{m}$ with a standard deviation of $6 \mu\text{m}$. Comparing values down a column gives an average tilt of $9 \mu\text{m}$ with a standard deviation of $2 \mu\text{m}$. Using the calculated equation of the plane,

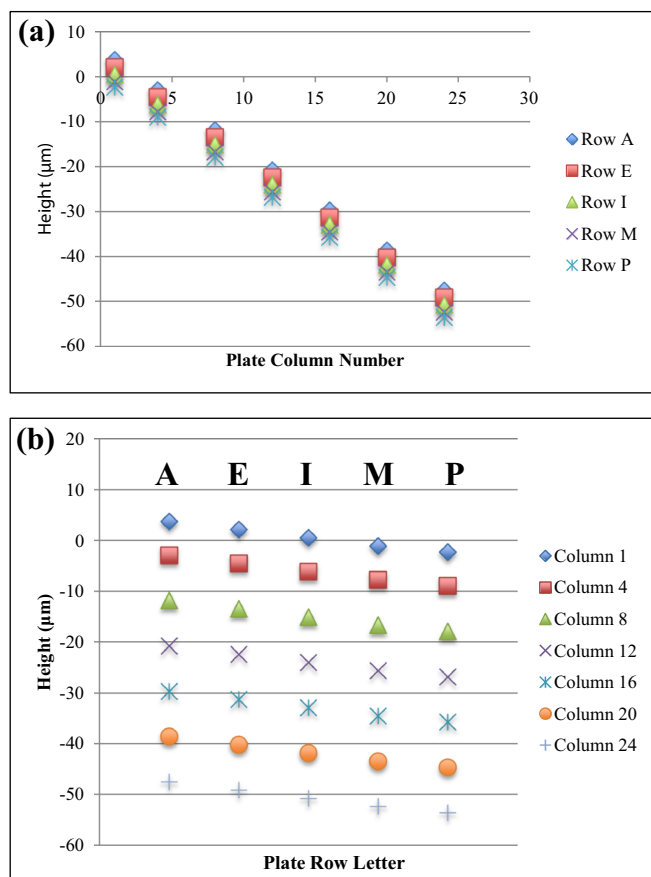


Figure 7. Plot of the calculated tilt of the sample stage (a) across a row and (b) down a column (rows A, E, I, P, and M) using the equation of the plane found for plate A

Table 6. Comparison of the Equation of the Plane Determined for Each Target Plate Used to Calculate the Tilt Across a Row and Down a Column of the Sample Plate, Which is Due to Misalignment of the Sample Stage

Plate	Equation of the plane	Tilt across a row (μm)	Tilt down a column (μm)
A	$z = -0.0004847x + 0.0001025y - 29.01$	50	7
B	$z = -0.0003943x + 0.0001387y - 23.60$	41	8
F	$z = -0.0005035x + 0.0001841y - 30.13$	52	12
M	$z = -0.0005311x + 0.0001246y - 31.79$	55	8
	Average	50	9
	SD	6	2

the tilt of the sample stage can be found using any of the plate shapes as demonstrated with the four plates in Table 6.

Using the method described here, in order to measure the tilt of the instrument sample stage, only the plate height measurements and laser images from a single sample plate are needed. Once the value of the tilt is determined across the rows and down the columns, adjustments can be made using the three-adjustment screws shown in Figure 1B. As the spacing between the threads on the screws is $\sim 0.40 \text{ mm}$, the required adjustment made to the screw is very small. Note that the current procedure to check the planarity of the stage for the Bruker Autoflex III requires samples be prepared and spotted on the four corners of the plate. Mass spectra are acquired from each of these samples; if the calculated mass error is over 200 ppm , the instrument is deemed to be out of specification. In this situation, the instrument would need to be brought up to atmosphere and then very fine adjustments need to be made to the three screws located in the source. The instrument would be put back under vacuum and these steps repeated until the error across the target plate is reduced sufficiently. Although the stage of our Bruker Autoflex III has yet to be adjusted, the advantage of the procedure described here is that only the laser images and plate height measurements are needed to correct the planarity of the stage. Images of the laser, easily taken at a few positions around the target plate, could be used to calculate the misalignment of the stage, eliminating the need for samples to check planarity. The instrument would not have to be repeatedly vented and evacuated to enable mass spectra to be taken, leading to a significant time savings in the stage adjustment process. Additionally, the laser images could be used to help improve the precision of commercial instruments through real-time adjustment of the sample stage along the z -axis if a motion control mechanisms were included in the instrument design.

Conclusion

A relationship between the image of the laser observed in the instrument sample-viewing camera and the position of the plate being sampled was observed. As the sample stage was moved to different sample positions, a very small but reproducible change in laser position was seen in relationship to the camera cross hairs. Using these movements of the laser, a method was developed to calculate the initial position of ion formation

along the z -axis. With the addition of a mechanism to control the position of the sample stage in the z direction, using this method to determine the z position using the laser image in the camera would allow the user control the position of ion formation and enable the improvement in mass accuracy and reproducibility of samples analyzed.

The measurement in the change in the initial position of the ion formation was used to develop corrections for TOF measurements made at different sample positions on the plate. The correction could be used for both peptide and synthetic polymer, and the measurement RSD was decreased from around 23 ppm to less than 6 ppm.

One application of this method for determining the plate height is to measure the misalignment of the sample stage of the instrument. Using the laser images and measured plate heights, a method was developed to calculate the misalignment of the sample stage. Using least squares fitting, an equation of the plane can be found and the height z can be calculated across and down a plate, yielding the tilt of the stage. Once this value is found, the sample stage can be physically adjusted using the three adjustment screws to align the sample stage. As demonstrated here, only one set of plate height measurements and z values are needed to determine the tilt of the instrument sample stage.

Acknowledgements

The authors thank the National Science Foundation for providing funding to purchase the Bruker Autoflex III MALDI TOFMS used in this work (NSF Grant No. 0840273). The authors also thank Mark Shiber from the Drexel University machine shop for the use of the Ames 412 depth gage.

Publisher's Note Springer Nature remains neutral with regard to jurisdictional claims in published maps and institutional affiliations.

References

1. Karas, M., Hillenkamp, F.: Laser desorption ionization of proteins with molecular masses exceeding 10,000 Daltons. *Anal. Chem.* **60**, 2299–2301 (1988)
2. Tanaka, K., Waki, H., Ido, Y., Akita, S., Yoshida, Y., Yoshida, T.: Protein and polymer analyses up to m/z 100 000 by laser ionization time-of-flight mass spectrometry. *Rapid Commun. Mass Spectrom.* **2**, 151–153 (1988)
3. Caprioli, R.M., Farmer, T.B., Gile, J.: Molecular imaging of biological samples: localization of peptides and proteins using MALDI-TOF MS. *Anal. Chem.* **69**(23), 4751–4760 (1997)
4. Rzagalinski, I., Volmer, D.A.: Quantification of low molecular weight compounds by MALDI imaging mass spectrometry – a tutorial review. *Biochim. Biophys. Acta, Proteins Proteomics.* **1865**(7), 726–739 (2017)
5. Trim, P.J., Snel, M.F.: Small molecule MALDI MS imaging: current technologies and future challenges. *Methods.* **104**, 127–141 (2016)
6. Chumbley, C.W., Reyzer, M.L., Allen, J.L., Marniner, G.A., Via, L.E., Barry, C.E., Caprioli, R.M.: Absolute quantitative MALDI imaging mass spectrometry: a case of rifampicin in liver tissues. *Anal. Chem.* **88**, 2392–2398 (2016)
7. Guilhaus, M.: Principles and instrumentation in time-of-flight mass spectrometry. *J. Mass Spectrom.* **30**, 1519–1532 (1995)
8. Malys, B., Piotrowski, M., Owens, K.G.: Diagnosing and correcting mass accuracy and signal intensity error due to initial ion position variations in a MALDI TOFMS. *J. Am. Soc. Mass Spectrom.* **29**(2), 422–434 (2018)
9. Hensel, R.R., King, R.C., Owens, K.G.: Electrospray sample preparation for improved quantitation in matrix-assisted laser desorption/ionization time-of-flight mass spectrometry. *Rapid Commun. Mass Spectrom.* **11**, 1785–1793 (1997)
10. Rasband, W.S.: ImageJ, U. S. National Institutes of Health, Bethesda, Maryland, USA, <https://imagej.nih.gov/ij/> (1997–2016) Accessed Oct 2017
11. Gobom, J., Mueller, M., Egelhofer, V., Theiss, D., Lehrach, H., Nordhoff, E.: A calibration method that simplifies and improves accurate determination of peptide molecular masses by MALDI-TOF MS. *Anal. Chem.* **74**, 3915–3923 (2002)
12. Moskovets, E., Chen, H., Pashkova, A., Rejtar, T., Andreev, V., Karger, B.L.: Closely spaced external standard: a universal method of achieving 5 ppm mass accuracy over the entire MALDI plate in axial matrix-assisted laser desorption ionization time-of-flight mass spectrometry. *Rapid Commun. Mass Spectrom.* **17**, 2177–2187 (2003)
13. Eberly, D.: Least squares fitting of data. (1999) Retrieved from <https://www.geometrictools.com/Documentation/LeastSquaresFitting.pdf> . Accessed June 2018.